Eur. Phys. J. D **38**, 427–438 (2006)
DOI: 10.1140/epjd/e2006-00050-2

THE EUROPEAN PHYSICAL JOURNAL D

Paramagnetic relaxation of spin polarized ^{3}He at bare glass surfaces

Part I

J. Schmiedeskamp[1,a], W. Heil[1,b], E.W. Otten[1], R.K. Kremer[2], A. Simon[2], and J. Zimmer[3]

[1] Institut für Physik, 55099 Mainz, Germany
[2] Max-Planck-Institut für Festkörperforschung, 70569 Stuttgart, Germany
[3] Schott AG Mainz, Germany

Received 26 August 2005 / Received in final form 19 December 2005
Published online 14 March 2006 –

Abstract. In this first in a series of three papers on wall relaxation of spin polarized, gaseous ^{3}He we investigate both by theory and by experiment surface-induced spin relaxation due to paramagnetic sites in the containing glass. We present experimental and theoretical evidence that — contrary to the traditional opinion — distant dipolar coupling to paramagnetic impurities in the glass, in particular iron ions, cannot be the dominant relaxation mechanism of ^{3}He-spins, although iron dominates the bulk static permeability. Instead dangling-bond type defects in the glass matrix are found to interact much stronger via the isotropic Fermi contact interaction. A model of paramagnetic site controlled ^{3}He relaxation including the Fermi contact interaction is presented. With reasonable semi-empirical assumptions our model allows to describe satisfactorily the measured relaxivities, both in the dissolution-dominated regime of fused silica or borosilicate glasses of the Pyrex type as well as in the surface dominated situation of aluminosilicate glasses which have only a low permeability for He atoms. In a large sample of 1.1 litre cells, built from various aluminosilicate glasses, an average relaxation time of 150 h is reached in case contaminant ferromagnetic particles have been demagnetized beforehand. From the maximum observed value of 250 h we derive after subtraction of dipolar relaxation in the gas phase a paramagnetic surface relaxivity of $\rho < 0.005$ cm/h at room temperature.

PACS. 33.25.+k Nuclear resonance and relaxation – 34.50.Dy Interactions of atoms and molecules with surfaces; photon and electron emission; neutralization of ions – 67.65.+z Spin-polarized hydrogen and helium

1 Introduction

New technologies for polarizing sizable quantities of ^{3}He up to high, non-equilibrium nuclear polarization have transformed this substance from a laboratory curiosity into a promising practical commodity. The common method to polarize ^{3}He gas in large quantities and with high yield is *Optical Pumping* [1–3]. There are two primary techniques to produce spin-polarized ^{3}He: (i) metastability exchange optical pumping (MEOP) [2] and (ii) Rb-spin exchange optical pumping (SEOP) [3]. The main breakthrough towards polarizing large quantities of ^{3}He gas to a high degree of polarization emerged with the development of powerful lasers operating at the required wavelengths [4,5] and — in case of MEOP — of techniques to compress the polarized gas free of relaxation to the high densities required [6].

For many applications like the use of spin-polarized ^{3}He as substitute of a target of polarized neutrons [7,8], polarized ^{3}He-based neutron spin filters for condensed-matter research [9–11] or the more recent application as contrast agent in lung diagnostics by Magnetic Resonance Tomography (MRT) [12–14], off-line operation of the polarizer is advantageous. Thus it is an essential issue to obtain long nuclear spin relaxation times T_1 in order to achieve and maintain large nuclear polarization of the samples. In case of storage containers relaxation times of several days are desirable for running experiments over longer periods or shipping the gas to more distant customers [15]. Typically the gas is polarized in glass tubes and stored in glass vessels; therefore our investigations concentrated on various types of glasses and their coatings.

[a] This paper comprises parts of the doctoral thesis of Jörg Schmiedeskamp; *present address*: Max-Planck-Institut für Polymerforschung, 55128 Mainz, Germany.

[b] e-mail: `wheil@mail.uni-mainz.de`

The most important relaxation source for ^{3}He spins usually results from their interaction with the walls of the glass container, provided the magnetic guiding field is sufficiently homogeneous [16] and the gas pressure does not exceed a few bars; the pressure dependent dipole-dipole interaction among the ^{3}He atoms limits the relaxation time to $(807/p)$ hours at room temperature where p is the ^{3}He pressure in bar [17]. In a series of three papers, referred to as Part I, Part II, and Part III, we present new experimental material and theoretical considerations on several types of wall relaxation of spin polarized ^{3}He: (i) paramagnetic relaxation at bare glass walls (Part I, this paper), (ii) paramagnetic relaxation at coated glass walls (Part II [18]), (iii) relaxation by small magnetized, ferromagnetic particles which occur as contaminants at the inner cell surface (Part III [19]). This research has led to a much better understanding and mastering of this complex matter. By now reliable procedures have been identified how to reach also in uncoated cells total relaxation times well above 100 h (including all sources of relaxation). This holds under the provision that any remanent magnetism of contaminant ferromagnetic particles inside the cells has been properly demagnetized.

Wall relaxation on bare glass surfaces which we treat in this first paper has been extensively studied by several groups in the past with the purpose to establish a reliable quantitative model of ^{3}He relaxation on glass surfaces. Fitzsimmons et al. [20] have pioneered this research giving a detailed insight into surface-induced nuclear-spin relaxation of gaseous ^{3}He including its temperature dependence. The basic mechanism of wall relaxation has been thought to be due to magnetic interaction with paramagnetic ions in the walls. The low-temperature scenario involves mainly ^{3}He adsorption on the glass surface, while at high temperature diffusion of ^{3}He into the glass bulk prevails for glasses with a more open network structure like, e.g., Pyrex and fused silica. The latter mechanism can be suppressed by using the more tightly packed and hence nearly impermeable glasses of the aluminosilicate type. As a result, long nuclear spin-relaxation times ($\geq$1 day) have been observed in such glasses like Corning 1720 or Schott Supremax. In a recent paper Jacob et al. [21] have refined this model, which is based on interactions with paramagnetic Fe^{3+} centres, with respect to solubility, diffusivity, and intrinsic relaxation of ^{3}He in the glass bulk. Under particular (though unrealistic, see below) assumptions on relevant correlation times they arrive at an improved quantitative description of ^{3}He wall relaxation in bare Pyrex glass.

In Section 2 we discuss the theory of paramagnetic sites controlled surface relaxation at permeable and impermeable glass walls. Beyond the usual distant dipolar coupling of the ^{3}He spins with paramagnetic iron impurity ions we take the much stronger Fermi contact interaction with dangling bonds into account. This aspect, so far, has not been considered in literature. In Section 3 we report on our experiences with uncoated cells manufactured from various glasses with different composition and chemical purity. Our experimental results challenge the common belief that iron impurities are the dominant source of paramagnetic relaxation. We also report here on our observations on the breakdown of relaxation times when ^{3}He cells have been exposed to the strong, magnetizing field of a tomography magnet, as well as on their recovery after proper demagnetization. These phenomena are thoroughly investigated in Part III. In Section 4 we give conclusions on the results presented in this article.

2 Theory of paramagnetic sites controlled ^{3}He relaxation at glass walls

2.1 Dipolar coupling of dissolved ^{3}He to distant iron impurities and dangling bonds

In the absence of ferromagnetic impurities paramagnetic impurity species in or on the walls provide the dominating relaxation mechanism of bottled nuclear polarized ^{3}He gas. In case of a permeable glass wall, ^{3}He atoms may be dissolved in the wall for some time, approach paramagnetic sites along the diffusion paths, relax, and finally re-enter the gas phase. In case of impermeable walls, paramagnetic relaxation can occur only while the ^{3}He atoms are adsorbed at the vessel surfaces. The most abundant paramagnetic impurity ion in commercial glasses is Fe^{3+}. For example, an analysis of their Fe_2O_3 content is given, e.g, by Timsit et al. [22] according to which iron ions are present in relative amounts of approximately 200 ppm in most of the glasses used. Hence, the current theories of which we give a brief critical review in this and the following subsection, have considered only relaxation on Fe^{3+} in case of glasses. The spin moments of the transition metal ions will depolarize a ^{3}He nuclear spin primarily through distant dipolar coupling (ddc). The average nuclear relaxation time of a ^{3}He atom dissolved in the glass at a distance r from a paramagnetic site is then [23]

$$\frac{1}{T_1^{ddc}} \approx \frac{6}{15}\frac{Q}{r^6}\frac{\tau_c}{1+\omega_0^2\tau_c^2}. \quad (1)$$

Here ω_0 is the ^{3}He Larmor frequency in the external field, and Q is the coupling constant with $Q = (\mu_0/4\pi)^2\gamma_{\mathrm{He}}^2\gamma_e^2\hbar^2 S(S+1)$. γ_{He} and γ_e are the gyromagnetic ratios in units of [rad/sT] for ^{3}He and the electrons, respectively. The spin of Fe^{3+} ions is $S = 5/2$. τ_c is the correlation time of the magnetic dipole-dipole interaction, which is limited by translational diffusion of the ^{3}He atoms with correlation time τ_{tr} and by spin-flips processes of the paramagnetic electrons with relaxation time τ_e. Following [24] they add up as rates according to

$$1/\tau_c = 1/\tau_{tr} + 1/\tau_e. \quad (2)$$

In the following we refer to reference [21], where predictions for the dissolution-controlled relaxation were made. It is shown that the relaxation of polarized ^{3}He in a bare glass cell can be written as the product of the surface to volume ratio A/V and a surface relaxivity ρ_{dis}^{ddc}. Throughout this paper we consider only the macroscopic surface to

Table 1. Solubility's and diffusivities for the glasses of interest, i.e., borosilicate (Pyrex), aluminosilicate glass (Supremax), and fused silica together with relevant values for $\tau_{\mathrm{Fe},0}$, $\tau_{defect,0}$, E_{Fe}, E'_D, etc. from bulk glass measurements or values extracted from this work [‡].

	Pyrex		Supremax		Fused silica	
S_0 [cm^{3}STP/cm^3]	$(6.3 \pm 0.6) \times 10^{-3}$	[29]	$(3.1 \pm 0.5) \times 10^{-3}$	[29]	$\sim 7.46 \times 10^{-3}$	[30]
E_S [eV]	0.015 ± 0.006	[29]	(0.029 ± 0.010)	[29]	-0.029 ± 0.003	[30]
D_0 [cm^2/s]	$(7.0 \pm 0.6) \times 10^{-4}$	[29]	$(1.8 \pm 0.3) \times 10^{-3}$	[29]	$\sim 3.04 \times 10^{-4}$	[30]
E_D [eV]	0.287 ± 0.005	[29]	0.59 ± 0.01	[29]	0.2413 ± 0.0025	[30]
$\tau_{\mathrm{Fe},0}$ [s]	$(1.9 \pm 0.2) \times 10^{-9}$	[24]	$(1.9 \pm 0.2) \times 10^{-9}$	[24]	—	—
$\tau_{def,0}$ [s]	—	—	—	—	$\sim 1.9 \times 10^{-9}$	[‡]
E_{Fe} [eV]	0.0351 ± 0.0031	[24]	0.0351 ± 0.0031	[24]	—	—
E'_D [eV]	—	—	—	—	~ 0.17	[24]
E_{def} [eV]	—	—	—	—	~ 0.114	[‡]
$\tau_{tr,0}$ [s]	—	—	—	—	$\sim 4.6 \times 10^{-12}$	[‡]
E_{ad} [eV]	~ 0.01	[27]	~ 0.01	[27]	~ 0.01	[27]
a_{dis} [Å]	5	[24]	5	[24]	3	[24]
a_{ad} [Å]	3	[24]	3	[24]	3	[24]
N^*_{Fe} [ppm]	~ 200	[22]	~ 200	[22]	—	—
N_{Fe} [m^{-3}]	$\sim 4 \times 10^{24}$		$\sim 4 \times 10^{24}$			
$N^*_{def,b}$ [ppm]	~ 0.5	[‡]	~ 0.5	[‡]	~ 0.5	[24]
$N_{def,b}$ [m^{-3}]	$\sim 10^{22}$		$\sim 10^{22}$		$\sim 10^{22}$	
$N_{def,s}$ [m^{-2}]	$\sim 5.4 \times 10^{15}$	[‡]	$\sim 5.4 \times 10^{15}$	[‡]	$\sim 5.4 \times 10^{15}$	[‡]
$\tau_{s,0}$ [s]	$\sim 2 \times 10^{-13}$	[‡]	$\sim 2 \times 10^{-13}$	[‡]	$\sim 2 \times 10^{-13}$	[‡]
V_0^{fci}/h [Hz]	1.97×10^{10}	[31]	1.97×10^{10}	[31]	1.97×10^{10}	[31]
b [Å^{-1}]	1.67	[31]	1.67	[31]	1.67	[31]

volume ratio as defined by the geometry of the cells. Relevant is the microscopic surface, however, which includes its roughness and which depends on the type of glass, its age and treatment. We have no means for measuring the microscopic structure of neither the inner cell surface nor its effect on the relaxation rate properly. Hence this has to be accounted for by treating the surface relaxivity as an effective parameter whose value is expected to scatter even.

Dissolution controlled surface relaxation shows a temperature dependence of Arrhenius type with the relaxivity constant ρ_0^{ddc} and the effective activation energy E_{eff}

$$\left(\frac{1}{T_{1,dis}}\right)^{ddc} = \frac{A}{V}\rho_{dis}^{ddc} = \frac{A}{V}S(T)\sqrt{D(T)\left\langle\frac{1}{T_1^{ddc}(T)}\right\rangle} = \frac{A}{V}\rho_0^{ddc}\exp\left(-\frac{E_{eff}}{kT}\right). \quad (3)$$

ρ_0^{ddc} can be determined from the ^{3}He-solubility in the bulk glass $S(T) = S_0\exp(-E_S/kT)$, its diffusion coefficient therein $D(T) = D_0\exp(-E_D/kT)$, and the effective relaxation rate $\langle 1/T_1^{ddc}(T)\rangle$ of the dissolved gas. The last term is obtained by integrating the effect of all paramagnetic ions on the ^{3}He nucleus from the distance of closest approach a_{dis} through all space

$$\left\langle 1/T_1^{ddc}\right\rangle = \int_{a_{dis}}^{\infty}(1/T_1^{ddc})N_e 4\pi r^2 dr. \quad (4)$$

Here $1/T_1^{ddc}$ is given by equation (1) and N_e is the density of paramagnetic centres in the glass. Since $\omega_0^2\tau_c^2 \ll 1$ holds, the shape of the spectral density $J(\omega_0) = \tau_c/(1+\omega_0^2\tau_0^2)$ (see Eq. (1)) reduces to $J(\omega_0) \approx \tau_c$. For Fe^{3+} in Pyrex and aluminosilicate glasses the correlation time τ_c is mainly limited by spin-flips on the paramagnetic ions [24], i.e., $\tau_c \approx \tau_{\mathrm{Fe}}$ with $\tau_{\mathrm{Fe}} = \tau_{\mathrm{Fe},0}\exp(E_{\mathrm{Fe}}/kT)$. In this case the relaxivity constant and the effective activation energy can be written as

$$\rho_0^{ddc} = \sqrt{\frac{24\pi}{45}\frac{N_{\mathrm{Fe}}Q}{a_{dis}^3}}S_0\sqrt{\tau_{\mathrm{Fe},0}D_0},$$
$$E_{eff} = E_S + (E_D - E_{\mathrm{Fe}})/2. \quad (5)$$

Different from ordinary glasses, high quality fused silica has considerably reduced iron content. Hence defects in the glass structure comprising broken Si–O bonds with unpaired electrons (dangling bonds) have been claimed responsible for ^{3}He relaxation in this case [24]. From ESR spectra the corresponding correlation time τ_{def} is measured to be $\approx 16 \times 10^{-8}$ s at room temperature ($t = 25$ °C) [24,25]. Thus τ_{def} is much larger than the correlation time for translational motion τ_{tr} which is approximately given by $\tau_{tr} \approx (\Delta r)^2/6D$. With the jump distance Δr of (2.5 ± 0.4) Å [24,26] it amounts to $\approx 0.5 \times 10^{-8}$ s at 25 °C (see Tab. 1). In order to give an estimate on τ_c (Eq. (2)) over the whole temperature range considered, we use the following ansatz: $\tau_e \equiv \tau_{def} = \tau_{def,0}\exp(E_{def}/kT)$ and $\tau_{tr} = \tau_{tr,0}\exp(E'_D/kT)$ with the assumption $\tau_{def,0} \approx \tau_{\mathrm{Fe},0}$. For E'_D one uses the activation energy extracted from the measured temperature dependence of $T_1(^3\mathrm{He})$,

$T_2(^3\mathrm{He})$ giving $E'_D = (0.186 \pm 0.021)$ eV [24]; this value is somewhat smaller than measured directly from diffusion. The parameters E_{def} and $\tau_{tr,0}$ can be determined from the measured values for τ_{def} and τ_{tr} at room temperature (25 °C), respectively, and are listed in Table 1.

In a first approach, defect-induced relaxation rates have been derived assuming distant dipole coupling of a defect spin of $S = 1/2$ to the ^{3}He nuclear spin according to equation (1) [23]. For the dissolution-controlled relaxation in fused silica one then obtains

$$\left(\frac{1}{T_{1,dis}}\right)^{ddc}_{quartz} = \frac{A}{V}\sqrt{\frac{24\pi}{45}\frac{N_{def}Q\,(S=1/2)}{a^3_{dis}}}S_0\sqrt{\tau_c\,(T)\,D_0} \times \exp(-(E_D/2+E_S)/kT). \quad (6)$$

Below we will also consider the stronger Fermi contact interaction. With this assumption we are able to significantly improve the description of the experimental results.

2.2 Relaxation of adsorbed ^{3}He

Adsorption of ^{3}He atoms on the glass surface in the neighbourhood of paramagnetic impurities has to be considered as a second source of relaxation. Helium is known to adsorb onto glass surfaces with adsorption energy of $E_{ad} \approx 0.01$ eV [27]. According to the Frenkel law [28] the sticking time per collision is related to E_{ad} by the expression

$$\tau_s = \tau_{s,0}\exp(E_{ad}/kT). \quad (7)$$

Here $\tau_{s,0} \approx 10^{-13}$ s is the high temperature limit representing the duration of a simple reflection of incident gas atoms. The number n of gas atoms adsorbed at any instant is just the product of τ_s and the rate, at which atoms collide with the surface,

$$n = \frac{N_V\overline{v}A}{4V}\tau_s. \quad (8)$$

Here N_V is the number of ^{3}He atoms in a container of volume V and surface area A, and $\overline{v}$ is the mean thermal velocity of ^{3}He atoms ($\overline{v} = \sqrt{8kT/m\pi}$).

For the relaxation in a cell in which adsorption processes dominate Fitzsimmons et al. [20] derived a general expression for $T_{1,ad}$ without reference to a specific atom-surface interaction

$$\frac{1}{T_{1,ad}} = \frac{n}{N_V}\left\langle\frac{1}{T_1^{ddc}}\right\rangle_{ad}. \quad (9)$$

Here $\langle 1/T_1^{ddc}\rangle_{ad}$ is the effective relaxation rate of the adsorbed gas. Here we derive $\langle 1/T_1^{ddc}\rangle_{ad}$ in a similar way as it was done for the relaxation of dissolved gas (Eq. (4)). We use again equation (1) and integrate the effect of all paramagnetic ions in the glass on the ^{3}He atom which is adsorbed at distance a_{ad} from the surface

$$\left\langle\frac{1}{T_1^{ddc}}\right\rangle_{ad} = 2\pi\int_0^\infty\frac{6}{15}QN_e\tau_c r^2dr \times\int_0^{\pi/2}\frac{\sin\vartheta d\vartheta}{\left(a^2_{ad}+r^2+2a_{ad}r\cos\vartheta\right)^3} = \frac{\pi}{15}QN_e\frac{\tau_c}{a^3_{ad}} \cong \frac{\pi}{15}QN_e\frac{\tau_s}{a^3_{ad}}. \quad (10)$$

In case of adsorption-controlled relaxation, we have to take into account the fact that with the sticking time τ_s a third correlation time is involved, which is much shorter than the characteristic spin-flip times τ_{Fe} or τ_{def} and the correlation times τ_{tr} of diffusion, respectively. Thus, the total rate adds up to $1/\tau_c = 1/\tau_{\mathrm{Fe}(def)} + 1/\tau_{tr} + 1/\tau_s \approx 1/\tau_s$.

Substituting the expressions for $\langle 1/T_1^{ddc}\rangle_{ad}$, n, and τ_s into equation (9) the relaxation rate of adsorbed ^{3}He due to distant dipolar coupling is

$$\left(\frac{1}{T_{1,ad}}\right)^{ddc}_{I} = \frac{A}{V}\frac{\pi}{60}\bar{v}QN_e\frac{\tau^2_{s,0}}{a^3_{ad}}\exp(2E_{ad}/kT) = \frac{A}{V}\rho^{ddc}_{ad}. \quad (11)$$

A similar result has been obtained by Fitzsimmons et al. [20]. They assume that the adsorbed ^{3}He atoms see an effective rms local magnetic field $\sqrt{\langle B^2_{loc}\rangle}$ with the assumption of a weak interaction, that is $\gamma_{\mathrm{He}}\sqrt{\langle B^2_{loc}\rangle}\tau_s \ll 1$. In this limit, $(\gamma_{\mathrm{He}}\sqrt{\langle B^2_{loc}\rangle}\tau_s)^2$ is just the probability W of a nuclear spin flip per encounter with the surface; it is connected to the characteristic relaxation rate $\langle 1/T_1^{ddc}\rangle_{ad}$ by [23]

$$\left\langle\frac{1}{T_1^{ddc}}\right\rangle_{ad} = \frac{2W}{\tau_s} = \frac{2\left(\gamma_{\mathrm{He}}\sqrt{\langle B^2_{loc}\rangle}\tau_s\right)^2}{\tau_s}. \quad (12)$$

Finally by use of equations (8) and (9) they get

$$\left(\frac{1}{T_{1,ad}}\right)^{ddc}_{II} = \frac{1}{2}\frac{A}{V}\bar{v}\gamma^2_{\mathrm{He}}\left\langle B^2_{loc}\right\rangle\tau^2_{s,0}\exp(2E_{ad}/kT). \quad (13)$$

On closer inspection it is no surprise at that equations (11) and (13), apart from a numerical factor of order one, are identical if we take $\langle B^2_{loc}\rangle$ to be

$$\left\langle B^2_{loc}\right\rangle = \left(\frac{\mu_0}{4\pi}\right)^2 N_e 2\pi\int_0^\infty\int_0^{\pi/2}\frac{\mu^2_B g^2}{d^6}\sin\vartheta d\vartheta r^2 dr. \quad (14)$$

Here g is the g-factor of the Fe^{3+}-ion, μ_B is the Bohr magneton, and $d = (a^2_{ad}+r^2+2a_{ad}r\cos\vartheta)^{1/2}$. Since wall relaxation rates on aluminosilicate glasses are adsorption-dominated at room temperature, we can check here equations (11) and (13) separately from the dissolution-controlled term (Eq. (6)). Using the parameter values

listed in Table 1, for example, equation (11) yields an adsorption-controlled relaxivity by Fe^{3+} impurity ions of $\rho_{ad}^{ddc} = (1/T_{1,ad})_I^{ddc} V/A \cong 2.2 \times 10^{-7}$ cm/h. This result, however, underestimates the measured paramagnetic surface relaxivity of aluminosilicate glasses of $\rho \approx 0.005$ cm/h (Sect. 3.3) by more than three orders of magnitude[1]. The discrepancy between theory and experiment has been discussed already in reference [20]: in order to match experimental results one would be forced to raise drastically the effective microscopic relaxing area beyond the macroscopic geometrical area and/or the characteristic sticking time $\tau_{s,0}$ beyond the generally accepted fundamental lattice-vibration period of $\sim 10^{-13}$ s (see Eq. (7)). Timsit et al. [22], to whom subsequent publications like, e.g., reference [21] refer, adopt in their different derivation of ρ_{ad}^{ddc} still the correlation time as it is used for dissolution-controlled relaxation, namely $\tau_c \approx \tau_{\mathrm{Fe}}$ instead of the much shorter τ_s. This way they meet the right order of magnitude of ρ, indeed, since equation (11) is now boosted by a factor $\sim \tau_{\mathrm{Fe}}/\tau_s$ (see Tab. 1). But the question remains how this assumption can be justified. Summarizing we conclude that the iron content in ordinary glasses cannot be claimed any longer to be the dominant source of adsorption-controlled surface relaxation of ^{3}He. At that point we remark that we have been triggered to revisit the theory by our corresponding preceding experience with glasses of different iron content (see Sect. 3.4).

2.3 Relaxation by paramagnetic dangling bonds due to Fermi contact interaction

The result of the preceding section forces us to search for a stronger relaxation mechanism than the distant dipole interaction. In the following we reconsider the case of dangling bonds whose unpaired electron belongs to the valence shell and may interact with a neighbouring ^{3}He atom through a σ-bond. Hence the electronic spin should couple to the nuclear spin through the much stronger Fermi contact interaction (fci). In the following we present an extension of the ^{3}He relaxation model to that case.

Dangling-bond types of defects have been most thoroughly studied at (111) Si/SiO_2 surfaces by means of electron spin resonance techniques [32]. Up to 0.5% of the (111) surface silicon atoms are not bonded to an oxygen atom of the oxide and there are numerous recipes how to remove these paramagnetic interface defects both by chemical and thermal treatments. Thus, there are good reasons to believe that not only in fused silica but also in other glasses like Pyrex, Supremax, etc. dangling-bond type defects exist up to certain concentrations [33], although in the latter case quantitative numbers cannot be extracted directly from ESR measurements due to the dominance of Fe^{3+} paramagnetic impurities in the bulk material. In the following we denote with $N_{def,b}$ the defect density in the bulk material (glass network) and, correspondingly, $N_{def,s}$ the area density of defects at the surface. We can then start from equation (12) and determine the intrinsic relaxation rates $\langle 1/T_1^{fci}\rangle_{dis}$ and $\langle 1/T_1^{fci}\rangle_{ad}$ for dissolution- and adsorption-controlled relaxation, respectively, by calculating the local hyperfine field B_{loc} from *fci* instead of *ddc*. Spin exchange rates associated with *fci* have been extensively studied between optically pumped alkali atoms and noble-gas nuclei [31,34,35]. Hence we may use here tentatively the same interaction potential as found, e.g., in the Rb–^{3}He system

$$V^{fci}(r) = hA^{fci}(r)(\hat{I}\cdot\hat{S}). \tag{15}$$

Walker et al. [31] have calculated $V^{fci}(r)$ which for $r \geq 2$ Å can be approximated by the expression $V^{fci}(r) \cong V_0^{fci}\exp(-br)$ with the strength constant V_0^{fci}/h to be 1.97×10^{10} Hz and the reach constant b to be 1.67 Å^{-1} (h in Eq. (15) is the Planck-constant).

If we now replace in equation (12) $\tau_s(T)$ by $\tau_c(T)$ and furthermore the expression in parentheses by $2\pi(V^{fci}(r)/h)\tau_c(T)$ we can calculate the dissolution-controlled intrinsic relaxation rate $\langle 1/T_1^{fci}\rangle_{dis}$ analogous to equation (4)

$$\begin{aligned}\left\langle \frac{1}{T_1^{fci}} \right\rangle_{dis} &= \int_{a_{dis}}^{\infty} 2\left(2\pi V^{fci}(r)/h\right)^2 \tau_c(T) N_{def,b} 4\pi r^2 dr \\ &= 32\pi^3 N_{def,b}\left(V_0^{fci}/h\right)^2 \tau_c(T)\exp\left(-2ba_{dis}\right) \\ &\quad\times\left(\frac{a_{dis}^2}{2b}+\frac{a_{dis}}{2b^2}+\frac{1}{4b^3}\right).\end{aligned} \tag{16}$$

Finally, by inserting this expression into equation (3) we get a quantitative prediction for the dissolution-based relaxation $(1/T_{1,dis})^{fci}$ due to Fermi-contact interaction

$$\left(\frac{1}{T_{1,dis}}\right)^{fci} = \frac{A}{V}S(T)\sqrt{D(T)\left\langle\frac{1}{T_1^{fci}(T)}\right\rangle_{dis}} = \frac{A}{V}\rho_{dis}^{fci}. \tag{17}$$

It should be noted that the temperature dependence of $(1/T_{1,dis})^{fci}$ will be the same as for $(1/T_{1,dis})^{ddc}$ or $(1/T_{1,dis})_{quartz}^{ddc}$ in the case of fused silica, since the same expressions are used for the respective correlation time $\tau_c(T)$, the diffusion coefficient $D(T)$, and the solubility $S(T)$.

In a similar way one can find an expression for the intrinsic adsorption-controlled relaxation rate

$$\begin{aligned}\left\langle \frac{1}{T_1^{fci}} \right\rangle_{ad} &= \int_{0}^{\infty} 2\left(2\pi V^{fci}(d')/h\right)^2 \tau_s(T) N_{def,s} 2\pi r dr \\ &= 4\pi^3 N_{def,s}(V_0^{fci}/h)^2 \tau_s(T)\exp(-2ba_{ad}) \\ &\quad\times\left(\frac{1+2ba_{ad}}{b^2}\right).\end{aligned} \tag{18}$$

[1] Strictly speaking, the measured value has to be considered as an upper limit; but we have reason to expect the right value not too far from it and take it as such in the following.

Here d' is given by $d' = \sqrt{a_{ad}^2 + r^2}$; the integral is taken over the surface only[2]. Finally by use of equations (9) and (8) we obtain for the adsorption-controlled relaxation rate

$$\left(\frac{1}{T_{1,ad}}\right)^{fci} = \frac{A}{V}\pi^3 \bar{v} \left(V_0^{fci}/h\right)^2 N_{def,s} \frac{1+2ba_{ad}}{b^2} \times \exp(-2ba_{ad})\tau_{s,0}^2 \exp(2E_{ad}/kT) = \frac{A}{V}\rho_{ad}^{fci}. \quad (19)$$

We may then add up the 4 different relaxation rates of equations (3), (11), (17), and (19) to arrive at a general expression for paramagnetic ^{3}He relaxation

$$\left(\frac{1}{T_1}\right)_{para} = \frac{A}{V}\left\{\left(\rho_{dis}^{ddc} + \rho_{ad}^{ddc}\right) + \left(\rho_{dis}^{fci} + \rho_{ad}^{fci}\right)\right\} = \frac{A}{V}\left\{\rho^{ddc} + \rho^{fci}\right\}. \quad (20)$$

2.4 Predicted surface relaxation on fused silica, aluminosilicate glass, and borosilicate glass (Pyrex)

Let us remark first that the *fci*-based equation (19) seems to yield now realistic numbers for the parameters $N_{def,s}$ and $\tau_{s,0}$, if we insert on the right side our measured surface relaxivity of aluminosilicate glasses of $\rho \approx 0.005$ cm/h (Sect. 3.3). We then obtain $N_{def,s}\tau_{s,0}^2 = 2.14 \times 10^{-10}$ s^2/m^2 for $a_{ad} = 3$ Å. This may be decomposed for example into $\tau_{s,0} \approx 2 \times 10^{-13}$ s and $N_{def,s} \approx 5 \times 10^{15}$ /m^2, which reproduce fairly well the expected numbers for $\tau_{s,0} (\approx 10^{-13}$ s) and $N_{def,s} \leq 10^{16}$/m^2 [32,33]. A still more quantitative experimental proof of equation (19) is found in the adsorption-controlled relaxation of ^{3}He, which has been measured in cells made from pure silicon single crystals [36]. The observed relaxation times of typically ≈1 hour would correspond to a surface defect density of $N_{def,s}^{Si} \leq 10^{18}$/m^2, a number which is supported by ESR measurements.

Next we like to include also the dissolution-controlled relaxation into the discussion. The two differ by the sign of their slopes in the Arrhenius plot. Due to the lack of experimental data, we set the dangling-bond type defect density $N_{def,b}$ in the network of aluminosilicate glass and borosilicate glass (Pyrex) to $N_{def,b} \approx 10^{22}$/ m^3 (∼0.5 ppm), the value reported for fused silica [24]. Vice versa, we adopt for fused silica and Pyrex as starting point of the discussion the same adsorption-controlled relaxivity $\rho_{ad} = 0.005$ cm/s as has been measured for aluminosilicate glass, i.e. the product term $N_{def,s}\tau_{s,0}^2 = 2.14 \times 10^{-10}$ s^2/m^2. All parameters entering the calculations are listed in Table 1.

In Figure 1 a number of theoretical relaxivities of ^{3}He, contained in bare fused silica cells, is plotted as a function of $1/kT$. The *ddc*-based relaxation by the paramagnetic

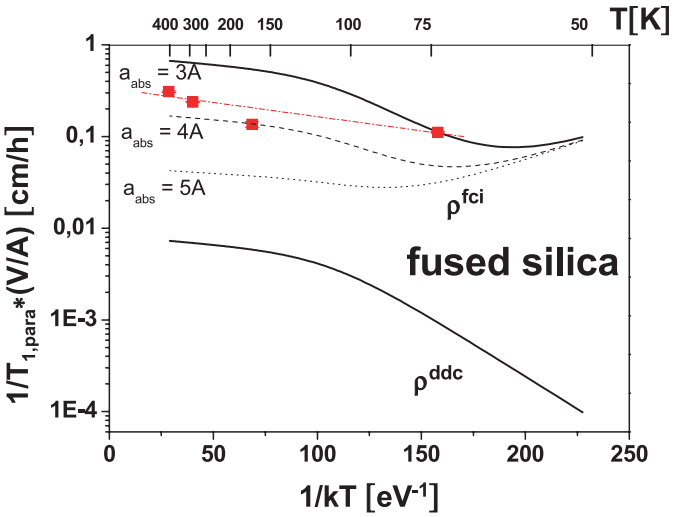

Fig. 1. Plot of calculated ^{3}He relaxivities $\rho = (V/A)/T_{1,para}$ versus $1/kT$ for fused silica glass. The corresponding temperature is given on the upper axis; ρ^{ddc}: distant dipolar coupling only; ρ^{fci}: including Fermi contact interaction for different closest distances of approach a_{dis}; squares: measured relaxivities with straight-line fitted to the data.

lattice defects, shown as ρ^{ddc} by the lower full line, falls by orders of magnitude below the measurements (solid squares) — the same finding as for the Fe^{3+}-relaxivity. A decisive increase in relaxivity is observed if the Fermi contact interaction with paramagnetic lattice defects is taken into account as shown by the upper curves in Figure 1, indicated as ρ^{fci}. Their slopes agree fairly well with the one of a straight line fit to the data points. In order to demonstrate the sensitivity on the distance of closest approach we varied a_{dis} in equation (17). The results are shown for 3 Å (upper solid line), 4 Å (dashed line), and 5 Å (dotted line). The data points lie in between the 3 Å and the 4 Å lines — a remarkable result, since it shows that some fine-tuning of the parameter-set suffices to reproduce the experimental data. The inclusion of the Fermi contact interaction obviously bridges the huge gap of missing relaxivity on fused silica, an open problem since long.

The quasi impermeable aluminosilicate glasses, like Supremax, the paramagnetic surface relaxation of which is dominated by adsorption, have to show a steady decrease of their relaxivity with increasing temperature at least up to 400 K. Figure 2 shows the theoretical result for ρ^{ddc} based on an iron content of 200 ppm. Since its adsorption component ρ_{ad}^{ddc} is orders of magnitude too low it is now clearly dominated by the opposite slope of a dissolution-controlled relaxivity ρ_{dis}^{ddc} for temperatures above 200 K already. On the other hand, the calculated values for ρ^{fci}, which have been normalized to our measured relaxivity of $\rho \approx 0.005$ cm/h at room temperature (full square), give a much stronger weight to adsorption-controlled relaxation because of the strongly enhanced defect concentration at the surface. Hence the full curve shows the expected temperature dependence, dominated by the Frenkel law (Eq. (7)).

[2] Integrating the effect of all defects in the bulk material ($N_{def,b}$) on the adsorbed ^{3}He atom shows that the corresponding relaxation rate is much less than $\langle 1/T_1^{fci}\rangle_{ad}$ of equation (18) using the parameters listed in Table 1.

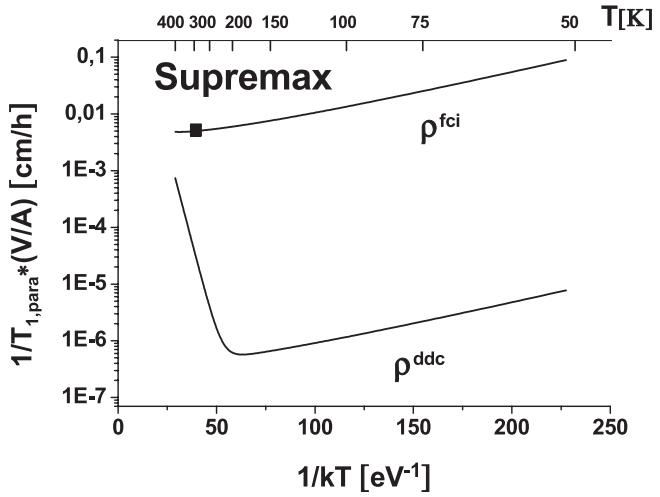

Fig. 2. Plot of calculated ^{3}He relaxivities $\rho = (V/A)/T_{1,para}$ versus $1/kT$ for Schott Supremax glass. The upper axis shows the corresponding temperature. For the relaxivity ρ^{ddc}, based on the distant dipolar coupling model, a Fe^{3+}-content of 200 ppm was assumed. The inclusion of dangling-bond type defects interacting via the Fermi contact term (ρ^{fci}) nicely reproduces the expected adsorption-dominated behaviour. Full square: measured paramagnetic relaxivity to which ρ^{fci} was normalized.

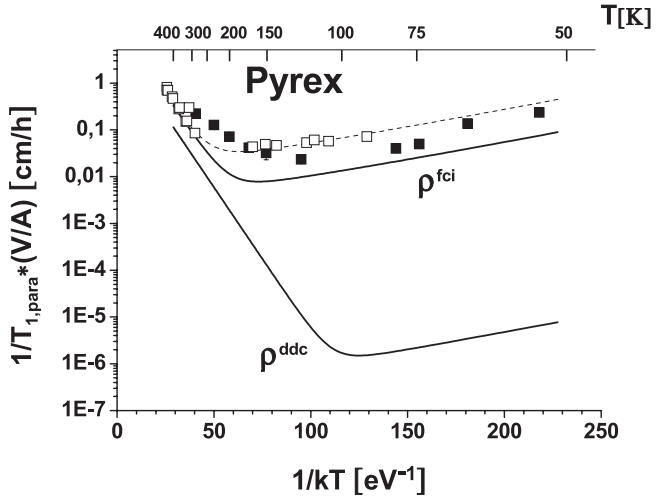

Fig. 3. Plot of calculated relaxivities ρ^{ddc} and ρ^{fci} (solid curves) versus $1/kT$ for Pyrex cells. The upper axis shows the corresponding temperature. For ρ^{ddc} the paramagnetic Fe^{3+}-concentration is again 200 ppm. The dashed curve shows the result for ρ^{fci} if $N_{def,s}\tau_{s,0}^2$ is increased by a factor of five over the value derived for Supremax glass (see text). Measured relaxivities taken from reference [21] (open squares) and reference [20] (solid squares).

The situation for Pyrex is similar in so far as ρ^{fci} dominates by far over ρ^{ddc} in the low temperature range (Fig. 3). Even at room temperature, in the dissolution-dominated regime, the contribution of the more frequent Fe^{3+}-ions (again set to 200 ppm) to the total surface relaxivity is of minor importance. All this is in agreement with our experimental findings for various glasses with different iron content. Our glass sample did not exhibit a clear correlation of the relaxivity on their iron content (see Sect. 3.4). Also shown are measured relaxation rates on Pyrex cells at different temperatures taken from reference [20] (solid squares) and reference [21] (open squares). Fortunately they cover the dissolution-controlled region at higher temperatures as well as the adsorption-controlled one at lower temperatures. In the former region the data are nicely matched by the relaxivity ρ^{fci} (solid line) which is calculated with the defect concentrations given above. At lower temperatures ρ^{fci} somewhat falls below the data points. One should keep in mind, however, that the decisive input parameter $N_{def,s}\tau_{s,0}^2$ of equation (19) has been fixed by normalization to our measured relaxivity on aluminosilicate glasses and then, in a first approximation, was assumed to be the same for the other glasses under investigation. Hence we may try for Pyrex a somewhat higher defect density at the surface, which also makes sense for this more open structured glass. As an example, the dashed curve in Figure 3 shows ρ^{fci} with the surface relaxivity increased by a factor 5. The data indicate that a factor in between 2 and 5 seems to be realistic. On the other hand such factors are well in the range by which the microscopic surface may exceed the geometrical one through roughness.

3 Relaxation times observed in uncoated glass vessels

3.1 Cell preparation and properties

The bulk of the material presented here concerns flasks of 1.1 litre storage volume. These were used for shipping polarized ^{3}He to various clinics for the purpose of lung imaging by MRT in the frame of the European network "PHIL" [37] during the years 2001 to 2004. The delay between polarization and application varied between 2 h and 24 h typically (a few days even, when the air carrier had lost the freight). Hence we were heading for relaxation times in the range of 100 h in uncoated cells, since the medical application excluded the presence of alkali metals.

For this purpose a total of 31 flasks were produced on special demand from iron-free aluminosilicate glasses by Schott AG Mainz, because in the beginning of the project we were still guided by the common opinion that iron would be the dominant source of nuclear relaxation in the glass vessels. High purity starting materials were selected for melts according to the chemical composition (see Tab. 2) of 3 commercial aluminosilicate glasses (3 flasks from Supremax glass, 12 from Corning 1720, and 16 from GE 180).

The flasks were blown from the melt into a mould of diameter 13 cm using a blowpipe from steel. At the given melt temperature of about 1500 °C there was no realistic chance for using any non ferrous pipe material, instead. Hence the pipe was covered by an electrolytic platinum layer at least in the region where it had contact with the melt in order to prevent dissolution of iron into the melt.

Table 2. Compositions of main glass types in wt% (only main components with an accuracy of 1%) Paramagnetic impurities ≈200 ppm [22].

Glass name	Duran	Supremax	GE 180	Corning 1720	Pyrex
Glass type	borosilicate	aluminosilicate	aluminosilicate	aluminosilicate	borosilicate
SiO_2	81	52	60	60	82
B_2O_3	13	2		6	12
Al_2O_3	2	22	14	17	2
Na_2O	3			1	4
K_2O	1			<1	
MgO		8		7	
CaO		7	7	9	
SrO			<1		
BaO		2	18	<1	
TiO_2			<1		
P_2O_5		8			

Fig. 4. Photograph of a 1.1 litre storage- and transport cell made from iron-free Corning 1720 glass produced on special demand by Schott AG Mainz.

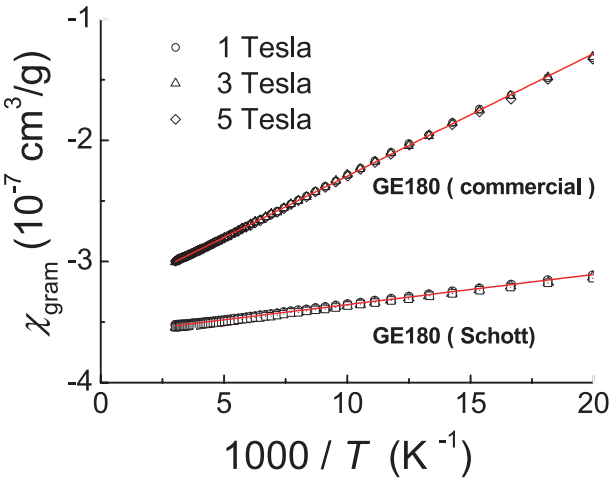

Fig. 5. Paramagnetic susceptibility per gram from iron-free GE 180 glass (Schott) and commercial GE 180 glass versus $1/T$ measured in the temperature range $50 \leq T$ [K] ≤ 330 at constant fields of 1 T, 3 T, and 5 T.

Still small ferromagnetic steel or (more probably) rust particles may have been blown into the flasks (compare Part III). In case of the GE 180 melt the platinum layer on the tip of the pipe was missing. Finally a stopcock with a glass flange both made from Duran was connected to the neck of the flask. A photo of a flask is shown in Figure 4.

In order to get a quantitative estimate of paramagnetism, the magnetic susceptibilities of a cylinder ($m \approx 0.5$ g) from GE 180 glass (Schott special glass melt) and several pieces ($m \approx 0.25$ g) from commercial GE 180 glass tubes were measured in a MPMS SQUID magnetometer [38] at constant fields of 1 T, 3 T and 5 T in the temperature range 50 K $\leq T \leq$ 330 K.

As shown in Figure 5, for each individual measuring field and sufficiently high temperatures the susceptibilities ($\chi_g = M_g/B$) to a good approximation follow a Curie law $\chi_g = C_g/T + \chi_0$ with the first temperature dependent term arising from paramagnetic impurities and the temperature independent part χ_0 representing essentially the diamagnetic contribution χ_{dia} from the closed electronic shells. Both glass probes are clearly different in their amount of paramagnetic impurities indicated by the different slopes in the plot of χ_g versus $1/T$. If we attribute the paramagnetic contribution to Fe^{3+} ions with a $3d^5$ configuration and an effective spin-only moment of 5.9 Bohr magnetons (μ_B) corresponding to $S = 5/2$, the impurity concentrations amount to 139(1) ppm for the commercial GE180 glass and to 34(1) ppm for the special glass melt.

Supremax cells were first cleaned by Mucasol (Merz Consumer Care GmbH, Germany), a tenside and phosphate based purifying agent. Thereafter the cells were rinsed with distilled water and then baked out at ∼400 °C in vacuum ($p \approx 10^{-8}$ mbar) for three days. Corning 1720 cells were cleaned with ethanol in order to reduce the dissolution of metal ions from the glass surface. The same bake-out procedure as before was retained. In case of GE 180 glass we simplified our previous preparation procedure considerably in that the cells were only evacuated for 3 days without bake-out and preceding cleaning procedure. Furthermore, we observed that T_1 did not change if the GE 180 cells were repeatedly ventilated with air and then evacuated again. Grosso modo the relaxation times

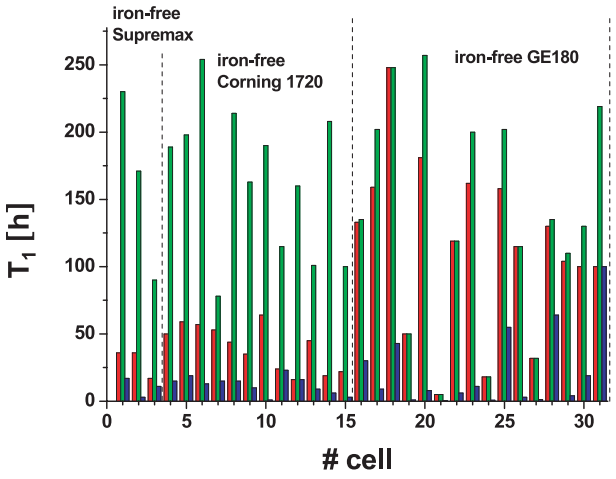

Fig. 6. Bar chart of measured T_1 times (error ±10%) in cells of iron-free Supremax (#1 to #3), iron-free Corning 1720 (#4 to #15), and iron-free GE 180 (#16 to #31). $T_{1,fresh}$: right after preparation (red bars), $T_{1,max}$: maximum observed value (green bars), $T_{1,min}$: minimum observed value (blue bars). In all cases a drop of T_1 is observed after exposure to a strong magnetic field (1.5 T). At the given conditions (^{3}He-pressure of 1 bar and room temperature) the dipolar relaxation by (^{3}He–^{3}He)-collisions contributes with a partial rate of (807 h)$^{-1}$; it has not been subtracted.

measured in GE 180 cells were comparable to those in cells manufactured from Supremax and Corning 1720 glass.

3.2 Phenomenology of observed relaxation times

The relaxation time of each flask has been checked many times in the course of its application for PHIL. The following standard procedure was applied: the flasks were filled with 1 bar of ^{3}He with a polarization degree of about 60%, delivered from our new MEOP polarizer [39][3]. The flasks were then placed into a magnetic field $B = 0.8$ mT of sufficient homogeneity (grad $B/B < 10^{-4}$ cm^{-1}) in order to suppress gradient relaxation. Nuclear resonance was excited automatically every 30 min at a small flip angle (about 10 mrad) and the free induction decay recorded. The destruction of nuclear polarization by the NMR pulses was proved to be negligible. The measurements were extended over periods long enough to allow for a reasonable fit of an exponential to the signal height. A relative error of 10% is estimated for all relaxation times quoted in this paper.

Figure 6 shows the measured relaxation times in freshly prepared cells ($T_{1,fresh}$, red bars). They scatter around an average of 40 h in case of iron-free Supremax and Corning 1720 cells and around an average of 110 h in case of GE 180 cells. But after they had returned from serving MRT purpose a serious breakdown of T_1 was observed usually. For a long time we considered this as being caused by some chemical contamination of the inner flask surface occurring during the administration of the gas to the patient (although the automatic administration unit developed for this very purpose [40–42] was furnished with a check valve). In many cases, indeed, a very significant reincrease of the relaxation time — even beyond the initial one — could be observed after applying another cleaning procedure within an ultrasonic Mucasol bath for 30 min at 80 °C before the flasks were evacuated and baked again at 400 °C.

It was only in 2004 that we realized that the exposure to the high magnetic field (1.5 T) of the MR tomography magnet induces the abrupt drop of relaxation times through the permanent magnetization of some ferromagnetic sites within the cells (compare Part III). This finding came as a surprise in so far as in the preceding paper on this effect by Jacob et al. [21] the ferromagnetic contamination was definitely attributed to ferromagnetic impurities of the Rb metal-coating. In all cases T_1 recovered after the cells had been demagnetized with a usual commercial demagnetizer for magnetic tapes. The commercial demagnetizer has been replaced later by a home made, larger instrument which was capable of covering the whole cell by a 50 Hz ac-field. Starting at maximum field amplitude of about 30 mT the field was then decreased manually to zero within a couple of seconds. This finding also leads us to suggest that the large increase of T_1 by the ultrasonic treatment of the cells may have happened as well through a demagnetization of ferromagnetic particles by the magnetostrictive action of the ultrasound vibrations. In addition, some ferromagnetic particles directly located at the glass surface may have been physically removed by the ultrasonic bath.

After proper demagnetisation the cells acquire an individual maximum of their relaxation time $T_{1,max}$ (green bars in Fig. 6). Their average of $\langle T_{1,max}\rangle = 150$ h attains a very satisfactory level although we observe still a significant scatter from 75 h to 250 h. We have also listed in Figure 6 the shortest relaxation time, $T_{1,min}$ (blue bars), ever observed in the magnetized state of an individual cell[4]. Their average has dropped to an unacceptable level of $\langle T_{1,min}\rangle = 17$ h. Also in freshly prepared cells relaxation is in the average by a factor of about 3 faster than in a properly demagnetized state. Apparently their magnetization has been sizeable already before exposure to high magnetic field (compare Part III). For the time being, we also hesitate claiming that we achieve reliably a complete demagnetization, although $T_{1,max}$ is fairly well reproduced by our new depolarizer in the meantime. Neither can we expect that the cells remain fully demagnetized in the weak field of about 1 mT of the optical pumping device until their T_1 is measured again. At present it is difficult to tell, therefore, whether the scatter in $T_{1,max}$

[3] At $P \approx 60\%$ the gas production of the Mainz MEOP polarizer reaches 3 bar litre/h.

[4] $T_{1,min}$ is not reproduced after each exposure to the tomography magnet, but scatters a lot. Apparently the cells do not leave the magnet of the tomograph always fully magnetized and with the magnetization vector in the same direction. This seems plausible, considering that they might have been turned around in the declining field during removal.

among the different cells represents different quality of the actual glass surface or still traces back to some residual relaxation by ferromagnetic sites (compare the test with a demagnetized soft iron piece inside a cell, described in Part III). If the latter applies, one may expect some correlation between $T_{1,max}$ and $T_{1,min}$ values. But this is not seen, except, possibly for GE 180 cells #21, #24, and #27 which may be regarded as heavily contaminated drop outs. This argument is based on their extraordinary low $T_{1,min}$ values of 0.5 h, 0.8 h, and 1.3 h, and correspondingly short $T_{1,max}$ values of 0.5 h, 18 h, and 32 h, respectively. One may speculate, whether this occurred because the blow pipe from steel was not covered with a platinum layer or any cleaning procedure was missing.

3.3 Paramagnetic relaxivity of aluminosilicate glasses

The above presented material proves that in our 1.1 litre sized iron-free, uncoated aluminosilicate glass cells relaxation rates of about 1/(250 h) can be achieved. However, the situation is still too complex as to allow for a straightforward determination of the paramagnetic relaxivity of these glasses from this number, because we cannot yet exclude safely any residual ferromagnetic contribution. To that end it would be necessary to clean up the fabrication process. So far we did not meet a single uncontaminated cell. Leaving aside this scruple one would interpret the scatter of $T_{1,max}$ values in Figure 6 as a measure of the typical scatter of the surface quality with respect to ^{3}He relaxation for this fairly large sample. On the other hand one may try to extract from the highest observed value, namely $T_{1,max} = (257 \pm 25)$ h measured in cell #20 from GE 180, a particular upper limit of the observed relaxivity. To that end we have to subtract first the rate of 1/(807 h) which originates from the dipolar relaxation at the given ^{3}He density and temperature [17]. Moreover we should consider the contribution from the small Duran surface in the neck. For the cell in question it amounts to $\approx$25 cm^2. Assuming here a typical relaxivity of 0.1 cm/h puts us into trouble, since only a negligible rate of 1/(16800 h) would be left over for the aluminosilicate glass itself. Hence we are forced to assume that these small Duran transition pieces actually relax less than usual (may be by some coverage from evaporated adjacent aluminosilicate; the joint has to be heated far beyond the ordinary blowing temperature of Duran). In fact, the surface area of the transition pieces varies between 3 cm^2 and 30 cm^2 but does not correlate to $T_{1,max}$. Hence we are not allowed to sharpen the limit by taking Duran relaxation separately into account but are left — strictly speaking — with an upper limit of 1/(430 h) for the paramagnetic surface relaxation rate for this particular GE 180 cell. This rate converts into a relaxivity of

$$\rho < 0.005 \text{ cm/h}. \tag{21}$$

Looking at the distribution of T_1 in Figure 6 we get the impression that the real value of ρ is probably not too far from this upper limit such that it makes sense to check theoretical models, at least, qualitatively against this observation (see Sect. 2).

3.4 Missing influence of iron content on paramagnetic relaxation

We have also collected some experience with glasses of ordinary iron content which lies typically in the range of (100–200) ppm, and we can compare the results to those obtained with so called iron-free glasses of "optical quality", whose iron content ranges around 30 ppm, usually (see Fig. 5). We first present the case of a 1 litre flask blown from a tube of ordinary GE180 glass ($\approx$130 ppm). The fresh flask showed an initial relaxation time of 130 h, which dropped to $T_{1,min} = 64$ h after magnetization in a 1.5 T field and attained a $T_{1,max} = 135$ h after demagnetization. The latter number almost meets the average of 150 h observed in iron-free flasks. Hence we do not recognise a clear influence of the iron content of this aluminosilicate glass on its ^{3}He relaxivity — at least not at the 100 ppm level.

Next we present a comparison of two commercial Duran glasses performed in prior, yet unpublished research [43]. In a series of 12 cells blown from ordinary Duran (Schott glass #8330) we measured an average relaxivity of $\rho(8330) = 0.14$ cm/h, whereas in 4 cells blown from the iron-free UV-Duran (Schott glass #4747) of "optical quality" we found an average of $\rho(4747) = 0.16$ cm/h, slightly, but insignificantly higher than in the ordinary glass. In these relatively fast relaxing cells we do not expect a dominant influence by — at the time yet undiscovered — magnetized impurities. But even if we select the cells with minimum relaxivity from both series $\rho_{min}(8330) = 0.093$ cm/h and $\rho_{min}(4747) = 0.125$ cm/h, the answer is the same: The iron is not found to be the dominant relaxant.

Finally we have checked four champagne bottles made of an ordinary soda lime glass, two from green and two from white glass. The colour stems from the addition of paramagnetic transition elements, mostly iron. After we had finished our T_1-measuring cycles, we took bore probes from the bottles and measured their magnetic susceptibilities as it was done before in case of GE 180 aluminosilicate glass. As a consistency check, the paramagnetism of fused silica (Suprasil) was measured, too (Fig. 7). From the slope of the Curie-law type susceptibility $\chi_g = (C_g/T) + \chi_0$ the spin concentrations were determined. If the paramagnetic contribution is attributed to Fe^{3+} ions with $S = 5/2$, we find concentrations of 4801 ppm for the green- and 530 ppm for the white glass samples. Otherwise their composition should be close to the standard glass composition (see Tab. 2). The measured iron impurities in fused silica give 0.12(7) ppm, as expected.

In order to use these bottles for ^{3}He storage their openings were grinded flat and connected through a flange to a stopcock, both made of Duran. The bottles were cleaned with Mucasol, rinsed with distilled water, evacuated for 1 day at room temperature, and finally filled with 1 bar of polarized ^{3}He. The first pair — a green and a white bottle — was measured before recognizing the risk of ferromagnetic contamination. We found $T_1 < 1$ h for the white and $T_1 = 22$ h for the green bottle. The second pair was measured quite recently: the white bottle was

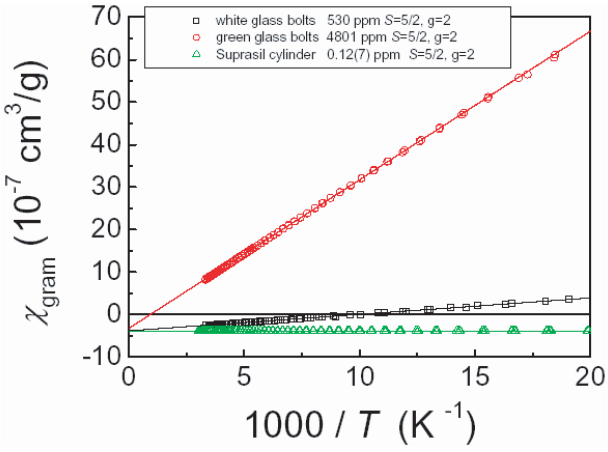

Fig. 7. Paramagnetic susceptibility per gram of two glass samples from champagne bottles (bore probes from green- and white-glass) and from a cylindrical Suprasil quartz glass sample versus $1/T$ measured in the temperature range $50 \leq T$ [K] ≤ 330 at constant fields of 1 T, 3 T, and 5 T. The slopes correspond to concentrations of 4800 ppm (green glass), 530 ppm (white glass), and 0.12(7) ppm (Suprasil) of Fe^{3+} ions with $S = 5/2$ spin-only moments.

measured before and after demagnetization. We found relaxation times of 1 h and 20 h, respectively. The green one was measured only after demagnetization and yielded a T_1 of 17 h. The magnetic field was sufficiently homogeneous over the length of the bottles as to neglect gradient relaxation. Summarizing we observe for demagnetized bottles a relaxation time of about 20 h irrespective of their colour. The number corresponds to a surface relaxivity of bottle glass of $\rho_{bottle} \approx 0.07$ cm/h slightly better than for Pyrex. Even at the elevated concentration of paramagnetic ions found for the green glass it seems that these still do not dominate the relaxation.

Particularly, these similarities of iron rich and iron poor glasses lead us to conclude that not only in pure fused silica but also in other glasses ^{3}He nuclear polarization relaxation is dominated by dangling bonds rather than by paramagnetic ions of transition elements, although the latter may be more frequent and dominate the bulk static paramagnetic susceptibility (compare Sect. 2).

Summarizing Section 3, we conclude that properly demagnetized aluminosilicate glass cells with fire polished surfaces as received from blowing, provide reliably relaxation times in excess of 100 h without any further surface coating or treatment. Thus they fulfil practical demands for storing and shipping polarized ^{3}He gas.

4 Conclusions

The traditional school of thought has accounted the relaxation of polarized ^{3}He stored in glass vessels to a paramagnetic iron content of the glass of the order 100 ppm. Accordingly we have fabricated vessels of 1.1 litre volume from several types of aluminosilicate glasses (Schott Supremax, Corning 1720, GE 180), molten from pure starting materials with an iron content depleted to less than 30 ppm. We have used these vessels extensively for storing and shipping polarized ^{3}He from our institute to Copenhagen (DK), Sheffield (UK) [15] and recently to Rochester (US) in the course of extended medical ^{3}He-MRI studies and collected ample experience on their relaxation properties. If properly demagnetized, we have observed relaxation times up to $T_1 = 250$ h. Corrected for other known relaxation sources one derives from this value a wall induced relaxation time of $T_{1,wall} \approx 430$ h, corresponding to a surface relaxivity as low as $\rho \approx 0.005$ cm/h. For the diffusion tight aluminosilicate glasses this has to be attributed to a surface interaction during adsorption only. Apart from this very satisfactory result, we have observed for a cell, blown from ordinary, iron containing Supremax glass, a T_1 in the same range as for the iron-free cells. So we have no proof that the Fe^{3+}-ions are really the relaxing agent. Identical relaxation times were also found in cells from ordinary and from iron depleted borosilicate glass (Schott Duran), where relaxation is dissolution dominated. Even in coloured ordinary bottle soda lime glass containing as much as 4800 ppm of iron in the paramagnetic state no sign of iron enhanced relaxation could be observed in comparison with ordinary white bottle soda lime glass.

Triggered by these results we have revisited the literature on the theory of ^{3}He relaxation in glasses. An early, still qualitative but valid treatment had already come to the conclusion that the contribution of Fe^{3+} to adsorption dominated relaxation should be negligible. But later, an explicit and thereafter generally accepted theory on Fe^{3+} relaxation managed to match the observed relaxation times. However, we find that this result has been obtained on the assumption of an unrealistically long correlation time of the distant dipolar hyperfine interaction between the ^{3}He nuclear and the Fe^{3+} electronic moment. Searching for an alternative explanation we have also revisited the relaxation by paramagnetic dangling bonds which are particularly frequent at glass surfaces. Such an attempt has been made already for the case of pure fused silica but on the basis of the much too weak distant dipolar coupling. Allowing for the Fermi contact interaction instead, we find by help of a semi-empirical calculation of its strength relaxation times which match the experimental results observed for fused silica. This holds also for glasses under reasonable assumptions on the density of dangling bonds in the bulk and at the surface.

This work was supported by the Innovationsstiftung Rheinland Pfalz under project number 539, by the Schott Glas Fonds of the company Schott AG, Mainz, and by the Deutsche Forschungsgemeinschaft in the frame of the Forschergruppe FOR 474.

References

1. A. Kastler, J. Phys. Radium **11**, 255 (1950)
2. F.D. Colegrove, L.D. Schearer, G.K. Walters, Phys. Rev. **132**, 2561 (1963)

3. M.A. Bouchiat, T.R. Carver, C.M. Varnum, Phys. Rev. Lett. **5**, 373 (1960)
4. G. Tastevin, S. Grot, E. Courtade, S. Bordais, P.J. Nacher, Appl. Phys. B **78**, 145 (2004)
5. I.A. Nelson, B. Chann, T.G. Walker, Appl. Phys. Lett. **76**, 1356 (2000)
6. J. Becker, W. Heil, B. Krug, M. Leduc, M. Meyerhoff, P.J. Nacher, E.W. Otten, Th. Prokscha, L.D. Schearer, R. Surkau, Nucl. Instr. Meth. A **346**, 45 (1994)
7. D. Rohe, P. Bartsch, D. Baumann, J. Becker, J. Bermuth, K. Bohinc, R. Böhm, S. Buttazzoni, T. Caprano, N. Clawiter, et al., Phys. Rev. Lett. **83**, 4257 (1999)
8. X. Zheng, K. Aniol, D.S. Armstrong, T.D. Averett, W. Bertozzi, S. Binet, E. Burtin, E. Busato, C. Butuceanu, J. Calarco, et al., Phys. Rev. C **79**, 065207 (2004)
9. R. Surkau, J. Becker, M. Ebert, T. Grossmann, W. Heil, D. Hofmann, H. Humblot, M. Leduc, E.W. Otten, D. Rohe, K. Siemensmeyer, M. Steiner, F. Tasset, N. Trautmann, Nucl. Instr. Meth. A **384**, 537 (1995)
10. W. Heil, K.H. Andersen, R. Cywinski, H. Humblot, C. Ritter, T.W. Roberts, J.R. Stewart, Nucl. Instr. Meth. A **485**, 551 (2002)
11. G.L. Jones, T.R. Gentile, A.K. Thompson, Z. Chowdhuri, M.S. Dewey, W.M. Snow, F.E. Wietfeldt, Nucl. Instr. Meth. A **440**, 772 (2000)
12. M.S. Albert, G.D. Cates, B. Driehuys, W. Happer, B. Saam, C.S. Springer, A. Wishnia, Nature **370**, 199 (1994)
13. M. Ebert, T. Grossmann, W. Heil, E.W. Otten, R. Surkau, M. Leduc, P. Bachert, M.V. Knopp, L.R. Schad, M. Thelen, The Lancet **347**, 1297 (1996)
14. K. Gast, B. Eberle, J. Schmiedeskamp, H.U. Kauczor, Acad. Rad. **10**, 1119 (2003)
15. E.J.R. van Beek, J. Schmiedeskamp, J.M. Wild. M.N.J. Palay, F. Filbir, S. Fichele. F. Knitz, G.H. Mills, N. Woodhouse, A. Swift, W. Heil, M. Wolf, E. Otten, Eur. Radiol. **13**, 2583 (2003)
16. L.D. Schearer, G.K. Walters, Phys. Rev. **139**, 1398 (1965)
17. N.R. Newbury, A.S. Barton, G.D. Cates, W. Happer, H. Middleton, Phys. Rev. A **48**, 4411 (1993)
18. A. Deninger, W. Heil, E.W. Otten, M. Wolf, R.K. Kremer, A. Simon, Eur. Phys. J. D **38**, 439 (2006)
19. J. Schmiedeskamp, H.J. Elmers, W. Heil, E.W. Otten, Yu. Sobolev, W. Kilian, H. Rinneberg, T. Sander-Thömmes, F. Seifert, J. Zimmer, Eur. Phys. J. D **38**, 445 (2006)
20. W.A. Fitzsimmons, L.L. Tankersley, G.K. Walters, Phys. Rev. **179**, 156 (1969)
21. R.E. Jacob, B. Driehuys, B. Saam, Chem. Phys. Lett. **370**, 261 (2003)
22. R.S. Timsit, J.M. Daniels, A.D. May, Can. J. Phys. **49**, 560 (1971)
23. N. Bloembergen, E.M. Purcell, R.V. Pound, Phys. Rev. **73**, 679 (1948)
24. R.K. Mazitov, P. Diehl, R. Seydoux, Chem. Phys. Lett. **201**, 543 (1993)
25. M.J. Mombourquette, W.C. Tennant, J.A. Weil, J. Chem. Phys. **85**, 68 (1986)
26. J.S. Masaryk, R.M. Fulrath, J. Chem. Phys. **59**, 1198 (1973)
27. D. Müller, Z. Phys. **188**, 326 (1965)
28. J. Frenkel, Z. Phys. **26**, 117 (1924)
29. A. Suckow, P. Schlosser, H. Rupp, R. Bayer, Glass Technol. **31**, 160 (1990)
30. D.E. Swets, R.W. Lee, R.C. Frank, J. Chem. Phys. **34**, 17 (1961)
31. T.G. Walker, W. Happer, Rev. Mod. Phys. **69**, 629 (1997)
32. The Physics and Chemistry of SiO_2 and the Si-SiO_2 Interface, *Symposium Proc. of the Electrochemical Society* edited by C.R. Helms, B.E. Deal (Plenum Press, 1988)
33. D.L. Griscom, J. Non-Crys. Sol. **73**, 51 (1985)
34. R.M. Herman, Phys. Rev. A **137**, 1062 (1965)
35. T.G. Walker, Phys. Rev. A **40**, 4959 (1989)
36. W. Heil, J. Dreyer, D. Hofmann, H. Humblot, E. Lelievre-Berna, F. Tasset, Physica B **267-268**, 328 (1999)
37. `www.phil.ens.fr`
38. MPMS (Magnetic Property Measurement System), Quantum Design, San Diego, CA 92121, USA
39. J. Schmiedeskamp, Ph.D. thesis, University of Mainz, 2005
40. L. Lauer, Diploma thesis, University of Mainz, 1997
41. B. Eberle, N. Weiler, K. Markstaller, R. Surkau, H.U. Kauczor, W.G. Schreiber, T.P.L. Roberts, W. Heinrichs, E.W. Otten, M. Thelen, J. App. Physiol. **87**, 2043 (1999)
42. F. Filbir, Diploma thesis, University of Mainz, 200
43. A. Deninger, Diploma thesis, University of Mainz, 1997